JOURNAL OF CATALYSIS 92, 312–326 (1985)

A Study of the Nickel-Catalyzed Methanation Reaction

R. E. HAYES,[1] W. J. THOMAS,[2] AND K. E. HAYES*

*School of Chemical Engineering, University of Bath, Bath BA2 7AY, England, and *Department of Chemistry, Dalhousie University, Halifax, Nova Scotia B3H 4J3, Canada*

Received January 25, 1984; revised June 15, 1984

A variety of chemical and physical techniques have been employed to investigate the nickel-catalyzed reaction between CO and H_2. The accumulated evidence suggests that CH_4 is produced by the stepwise addition of H_2 to surface carbon, which is formed by the dissociative adsorption of CO. The rate determining step is the formation of Ni≡C—H complex. Catalytic deactivation of Ni catalysts prepared by impregnation is reversible. The original activity can be regained by hydrogenation at temperatures higher than those employed for methanation. Catalysts prepared by coprecipitation exhibited irreversible deactivation. The deactivation process appears to be a result of phase transformation of surface carbon. Highly structured carbon is not produced under methanation conditions. Addition of Pt or Ru to Ni supported catalysts sustains and improves catalytic activity. The rate of catalytic methanation is best described by means of a kinetic power law.

INTRODUCTION

Interest in the nickel-catalyzed reaction between carbon monoxide and hydrogen has been prominent ever since the initial investigations of Sabatier and Senderens (*1, 2*). Prior to the availability of copious supplies of natural gas, methane was made commercially by reacting carbon monoxide and hydrogen, both reactants deriving from the pyrolysis of coals with subsequent gas processing. Although the manufacture of methane on a large scale virtually ceased following the discovery and economic distribution of natural gas, the methanation reaction was employed in ammonia processing plants for the removal of small quantities of carbon monoxide from ammonia synthesis gas. For this purpose a 20–25 wt% nickel (expressed as NiO) catalyst supported on alumina operating at 300–350°C and any pressure (depending on downstream plant requirements) ranging from 1 to 300 bar is adequate (*3*). With the continually increasing cost of natural gas, however, the catalyzed reaction of carbon monoxide, and also carbon dioxide, with hydrogen is becoming a more economically attractive source of methane, especially as synthesis gas processes based on fossil fuels are adopted. Concentrations of reactants in synthesis gas plants are very much greater than in plants which remove carbon monoxide during ammonia processing and consequently the fast exothermic methanation reaction is better accomplished with a catalyst containing a lower nickel loading (*ca.* 10–15 wt% NiO on alumina) and in reactors in which a considerable fraction of the product gas is recycled. Catalyst deactivation can occur by the formation of carbidic precursors which can rapidly lead to undesirable carbon deposition (*4*) and so conditions during start up and operation must be carefully controlled. For this reason knowledge of the deactivation process and reaction mechanism is of considerable importance.

Two types of mechanistic models are currently in favor and have been reviewed

[1] Present address: Technical University of Nova Scotia, Halifax, Nova Scotia, B3J 2X4, Canada.

[2] To whom correspondence should be addressed.

0021-9517/85 $3.00

(*5*). Thus, models involving the formation of surface complexes containing oxygen have been proposed (*5–7*) as well as the earlier model of Fischer and Tropsch (*8*), recently resurrected in differing forms (*9, 10*), which purports that the reaction proceeds through active surface carbon as an intermediate formed by the dissociative chemisorption of carbon monoxide. Whether or not the intermediate active surface carbon is carbidic or other forms of active carbon are produced by the dissociation of carbon monoxide (*11–13*), is still open to question. Several investigators employing an infrared technique have asserted that carbon monoxide chemisorbs on transition metals in both a bridged form, requiring two adjacent metal sites, and a linear form occupying a single site (*14*). Some recent theoretical and experimental work (*15, 16*) casts doubt on the existence of the bridged chemisorbed form. The adsorbed state of carbon monoxide is also influenced by the presence of adsorbed hydrogen (*17*), the proportion of bridged and linearly adsorbed CO depending on the nature of the adsorbent metal. Blyholder and Neff (*18*) noted the existence of species such as M–CH_2R at the surface of a silica-supported iron catalyst when it was heated in the presence of mixtures of CO and H_2, whereas King (*19*) observed only CH_2 groups. At the surface of a ruthenium catalyst both hydrocarbon and formate groups were observed (*20, 21*), although these were considered to be adsorbed products of reaction.

Araki and Ponec (*12*) employed isotopically labeled carbon to demonstrate that at methanation temperatures, surface carbon is produced by the dissociative adsorption of CO which can then be hydrogenated to CH_4 by addition of hydrogen. The question of the origin and significance of carbon deposition on the catalyst surface is obviously important in view of deactivation effects which have been observed (*22, 23*). Kinetics of the nickel-catalyzed methanation reaction are equally ambiguous, the models proposed by different authors (*24, 25*) satisfying a simple correlation in which the reaction rate is proportional to the partial pressure of carbon monoxide and the square root of the partial pressure of hydrogen (*26*). Vannice (*27, 28*) conducted an extensive investigation of catalytic methanation for a wide variety of metals and concluded that a kinetic power law in which the exponent of the carbon monoxide partial pressure is negative and that for the partial pressure of hydrogen is positive, is adequate to describe reaction rates.

We have applied a number of different techniques (described in this paper) to the problem of catalytic methanation in an attempt to elucidate the kinetics, deactivation, and mechanism of this industrially important reaction.

EXPERIMENTAL

The nickel-catalyzed methanation reaction was studied by employing a variety of experimental techniques to acquire information concerning the mechanism and kinetics of reaction and the catalyst deactivation process. Experimental methods used to study the catalyst surface and provide information about reaction mechanism included infrared reflectance and X-ray photoelectron spectroscopy and also scanning electron microscopy. A packed microreactor capable of operating at elevated pressures was used to study reaction rates and catalyst deactivation. This technique was also adapted to provide a means of perturbing inlet concentrations so that transient effects could be observed, thus yielding valuable information about the mechanism.

Catalyst Materials

The commercial catalyst (29% w/w Ni on γ-Al_2O_3) was supplied by I.C.I. Other catalysts employed were prepared in the laboratory by the incipient wetness technique and subsequently dried at 80–100°C and calcined at 500°C for 17 h. The desired metal was loaded on to 30–60 mesh sieved γ-Al_2O_3 by adding a measured volume of an aqueous solution of a known strength of the

appropriate salts $Ni(NO_3)_2$, $LaNO_3$, $RuCl_2$, AgCl, KNO_3 or H_2PtCl_6.

Surface area and pore size distribution of the fresh commercial and prepared catalysts were assessed by adsorption–desorption of N_2 at −196°C. Adsorption isotherms of both the commercial and prepared samples were of type IV (BET classification). Typical of the freshly prepared catalysts was a sample (9% Ni, 3% La) with a surface area of 258 $m^2\ g^{-1}$ and a wide sloping hysteresis loop ranging from 0.25 to 0.95 relative pressure. Following deactivation during methanation this same catalyst had a surface area of 157 $m^2\ g^{-1}$ and a sloping hysteresis loop from 0.55 to 0.90 relative pressure.

Prior to use the catalysts were reduced *in situ* under pure H_2 flowing at 60 $cm^3\ min^{-1}$ STP. One of three methods was employed, as follows: (a) the catalyst temperature was increased from ambient to 220°C at 5°C min^{-1}, held at 220°C for 1 h, and then raised at the same rate to 443°C and reduction continued for a further 22.3 h; (b) the same as (a), except that the temperature was held at 235°C and the final temperature was raised to 470°C; and (c) the same as (a), except that reduction at 443°C only lasted 3 h.

Catalytic Microreactor and Gas Analysis

The tubular microcatalytic reactor (50 mm depth by 9.5 mm bore) was of stainless steel and contained samples of up to 1 g of catalyst located between an inlet and outlet port separated by a vertical distance of 19 mm. The microreactor was capable of operation up to 1000 kPa and was mounted vertically. A thermocouple pocket enabled the temperature across the catalyst bed to be measured. Experimental measurements and calculations based upon material physical properties indicated that the temperature rise over the bed depth was always less than 1°C and the difference between actual and indicated temperature was no more than 2°C. A more detailed description of the microreactor and associated equipment has been given elsewhere (*29*).

Mass flow control valves and pressure gauges monitored and controlled the flow of gases to the reactor. Saturated water vapor could be added to the inlet when desired by passing a carrier gas through a thermostatted saturator. Gases and vapors were mixed before entry to the reactor by passage through a heated stainless-steel tube (15 cm length, 12 mm diameter) fitted with closely spaced baffle plates.

Products and reactants emerging from the microreactor were diverted through a four-way valve to a 2-cm^3 sample loop and then carried by He to a chromatographic unit consisting of three 2-m glass columns. Column 1 was packed with Carbosieve "S" and temperature programmed. The associated katharometer detected (in increasing order of retention times) H_2, N_2, CO, CH_4, H_2O, and CO_2. Quantities were obtained from peak areas after calibration, although analysis for H_2 was impracticable because of the multiple peak displayed when He is the carrier gas. Column 2 was operated at 100°C (with the katharometer detector at 150°C) and contained Chromosorb 102. This provided quantitative information about hydrocarbons (molecular mass > 16). Column 3 was packed with Poropak "Q" and served as a reference column to enable a steady baseline to be maintained throughout analyses.

Infrared analysis of the gas mixture from the microreactor served as an independent check on composition. The cell used (115 cm^3, 10 cm path) was fitted with gas inlet and exit and NaCl windows. For unsteady state experiments a different cell (15 cm^3, 5 cm path) was inserted in the product gas line, so that high purge rates could be attained. Calibration of infrared responses was obtained by passing pure gases together with diluent nitrogen through the cell. Preparation of many gas mixtures confirmed that there was less than a 2% difference between the results of analyses by

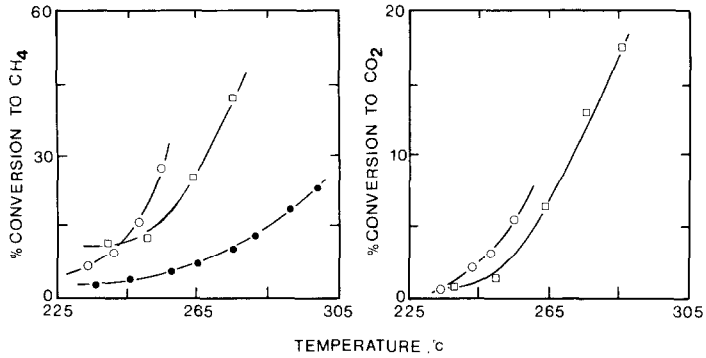

FIG. 1. Conversion of CO to CH_4 and CO_2 as a function of temperature. (□) Catalyst A; (○) Catalyst B; (●) Catalyst C.

gas–liquid chromatography and infrared spectroscopy.

Physical Characterization

Both the fresh and reacted catalysts were examined using scanning electron microscopy and X-ray photoelectron spectroscopy. A Jeol microscope (model 100 CX) equipped with an ASID high resolution scanning facility and an EDAX energy dispersive X-ray analysis system were used for viewing surfaces. Useful information concerning the reaction mechanism was obtained by computer enhanced multiple reflectance infrared spectroscopy. This latter technique, the spectrometer cells, metal plate preparation, and computer, have been described fully elsewhere (*16, 30, 31*). The nickel plates (2.00 mm thick) were machined from 99.9998% Ni and mechanically polished with alumina.

RESULTS

Catalyst Activity

Three differently prepared catalysts were employed to establish the conversion pattern of CO to CH_4 and CO_2. In these experiments 0.5 g of catalyst, uniformly diluted with 0.3 g of alumina to ensure thermal stability, was used. The reactor feed consisted of 3.1% CO and 9.3% H_2 (v/v) in diluent N_2, at a total flow rate of 410 cm^3 min^{-1} STP and a total pressure of 131 kPa. The results are illustrated in Fig. 1. Catalyst A was the 29% Ni commercial catalyst reduced by method (a), while catalyst B was the same catalyst reduced by method (c). Catalyst C was 9% Ni and reduced by method (a). It is clear that the commercial catalyst is much more active than the prepared catalyst, and that it is strongly influenced by the method of reduction. The commercial catalyst also produced much more CO_2 than the prepared catalyst. When the 9% Ni catalyst was reduced by method (b), no difference in activity was observed, as compared with reduction by method (a).

Initial activity and conversion as a function of time on stream (the length of time the catalyst is exposed to the steady flowing gas mixture) were measured for a series of promoted and unpromoted catalysts. Silver and platinum were selected as promoters because of their reported (*32*) hydrogen spill-over characteristics; potassium has been reported (*33*) as inhibiting graphitization, while mixtures of lanthanum and a noble metal have been observed to increase the hydrogenation of carbon (*22*). Ruthenium, on the other hand, is a recognised methanation catalyst (*17*). Typical of the deactivation occurring when promoted and unpromoted 9% Ni catalysts were employed are the curves illustrated in Fig. 2. Each deactivation displays an initial exponential decrease in activity with time, followed by a sharp transition to a more rapid

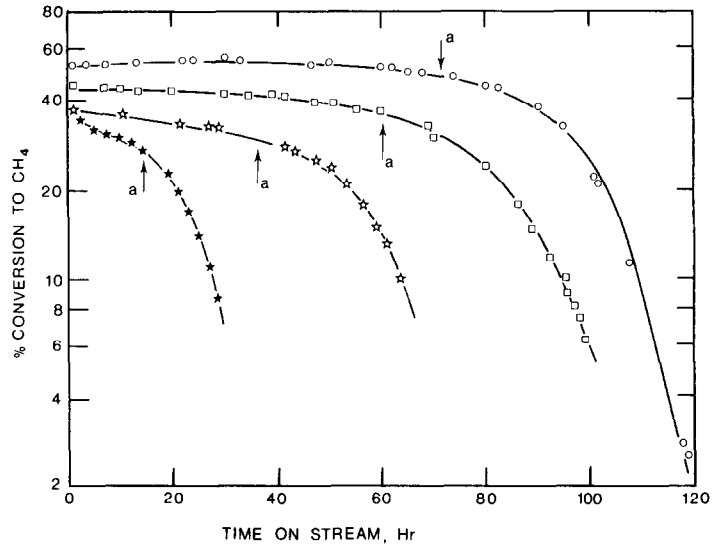

FIG. 2. Deactivation curves. (★) 9% Ni, Reduction method (b); (☆) 9% Ni, reduction method (a); (□) 0.9% Ru, 9% Ni, reduction method (a); (○) 1.5% Pt, 9% Ni, reduction method (a). Arrow 'a' indicates departure from linear deactivation.

decay (for convenience in presentation, the curves are plotted in semilogarithmic form).

These experiments were all performed over 0.5 g of catalyst at a constant temperature and pressure of 322°C and 131 kPa, respectively. The feed composition and flow rate were the same as for the previously described activity tests.

Of the promoters investigated, platinum and ruthenium significantly improved and sustained catalyst activity. Silver and potassium decreased both initial activity and lifetime, and while lanthanum yielded a marked increase in initial activity, it also caused very rapid deactivation. The choice of reduction method was also important, as catalysts reduced by method (a) had more sustained activity than those prepared by method (b). The initial activity and deactivation characteristics of all catalysts tested are summarized in Table 1.

For each catalyst, complete restoration of activity could be achieved by treatment with H_2 at 322°C, provided that deactivation had not progressed beyond the point at which rapid decay occurred (point a on each curve in Fig. 2). If deactivation had occurred to any greater extent, to restore initial activity the catalyst had to be heated to 450°C in flowing H_2 for 24 h.

The 29% Ni commercial catalyst exhibited an irreversible deactivation pattern when exposed to elevated temperatures during or after methanation. Figure 3 shows the effect of heating 0.5 g of catalyst to an elevated temperature in the presence of reactants for 15 min. The activity at selected methanation temperatures is seen to

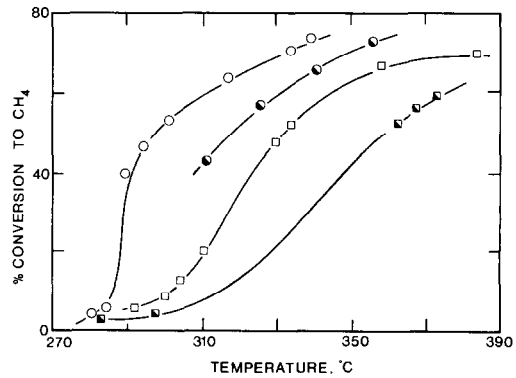

FIG. 3. Activity of a 29% Ni commercial catalyst, pre-heated in the presence of CO/H_2 mixture. (○) Pre-heated to 340°C; (◔) pre-heated to 360°C; (□) pre-heated to 390°C; (◪) pre-heated to 490°C.

TABLE 1

Summary of Initial Activities and Deactivation Characteristics of Catalysts

Catalyst composition (%)						Temp (°C)	Reduction method	Conversion to CH_4 (%)	Conversion to CO_2 (%)	Time to transition (h)	Time to 10% initial activity (h)
Ag	K	La	Ni	Pt	Ru						
			9			322	a	39.0	3.0	42.0	70
			9			322	b	38.0	3.2	16.0	30
		4	9			322	a	55.0	17.5	12.0	17
		4	9			322	b	55.0	17.0	4.0	6.5
		3	9			322	a	54.0	17.0	12.0	20
		3	9			300	a	28.0	3.0	18.0	40
		3	9			322	b	50.0	15.0	8.0	12
		2	9			322	a	52.0	12.8	22.0	32
		2	9			322	b	52.0	12.5	12.0	17
		4	9	2		322	a	62.0	24.0	3.3	6.5
		3	9	1.5		322	a	66.0	23.0	10.5	16
		2	9	1		322	a	60.0	16.0	15.0	25
			9	1.5		322	a	53.0	5.0	67.0	112
			9		0.9	322	a	47.0	7.0	60.0	100
	2		9			322	a	17.5	4.3	n/a	n/a
1			9			322	a	11.5	nil	n/a	n/a
		8				322	a	nil	nil	n/a	n/a
				1.5		322	a	3.3	nil	n/a	n/a

be reduced, the greatest activity loss occurring when the catalyst was heated to the highest temperature. Activity could not be restored by hydrogenation at temperatures up to 500°C. Oxidation of the catalyst surface with air produced CO_2, indicating the presence of carbon or hydrocarbon fragments on the surface. Rereduction after oxidation resulted in partial restoration of initial activity. In this series of experiments the reactor feed consisted of 7.4% CO and 22.2% H_2 by volume in N_2 at a total pressure of 131 kPa and total flow rate of 1020 $cm^3\ min^{-1}$ (measured at STP).

Kinetics

Of all the catalysts examined, only the 1.5% Pt, 9% Ni catalyst displayed a period of constant activity. This catalyst was therefore selected for the kinetic investigation. In the temperature range studied, *ca.* 260–300°C, the catalyst attained constant activity after 10 h, and sustained this activity for at least a further 60 h. Conversion of reactants was measured during this period of steady activity. Another advantage of this catalyst was the absence of any CO_2 in the product stream at temperatures below 300°C. As a result, modeling of the kinetics is simplified.

The reactor was operated as an integral reactor with differential analysis used to determine reaction rates. The range of process variables covered is given in Table 2. The experiments were designed so that the effects of each variable could be measured

TABLE 2

Range of Experimental Operating Conditions

Variable	Range covered
Catalyst mass	0.25–0.50 g
Temperature	260–300°C
Total flowrate	400–800 $cm^3\ min^{-1}$ (STP)
Total pressure	0.1–0.5 MPa
H_2/CO ratio	3–5
CO inlet concentration	3.2 vol%

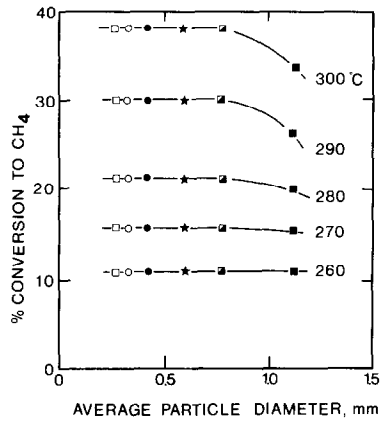

FIG. 4. Effect of catalyst particle size on conversion.

independently. Conditions were selected to ensure that both intra- and interparticle transport limitations were absent. Figure 4 describes the effect of particle size on conversion at several temperatures, measured at 100 kPa total pressure, H_2/CO ratio of 5, CO inlet concentration of 3.2 vol% and a total flowrate of 600 cm^3 min^{-1} STP. It is clear that, provided the diameter of the catalyst particles is less than 0.7 mm, diffusion within the porous pellet does not limit the conversion. In all experiments reported in this investigation, the catalyst size was 0.2–0.4 mm.

Figure 5 is typical of several experiments for the temperature range 260–300°C. It reveals that, for four differing masses of catalyst, conversion at a given temperature is a unique function of residence time within the reactor. The reaction is therefore not affected by interphase (gas to particle) transport. Calculations using the criterion of Mears (*34*) support the conclusion that mass transfer limitation from fluid to solid is absent for the experimental flow and temperature conditions employed.

The effect of product CO_2, H_2O, and CH_4 on the reaction rate was separately tested. In each test the inlet CO and H_2 partial pressures were constant, the H_2/CO ratio was 4, total pressure 100 kPa and temperature 270°C. The feed was 2.8% CO. The products were introduced by replacing a portion of the diluent N_2 stream with the appropriate product using a 3-way valve. When the feed contained 0.22 vol% CO or 0.73 vol% CH_4, no change in conversion of CO to CH_4 was observed; however, when the feed contained 2.6 vol% H_2O, the conversion fell from 22 to 18%, indicating reaction inhibition by H_2O. When the H_2O was removed from the feed stream, the conversion returned to 22%.

Some qualitative experiments were designed to introduce step changes in concentration of reactants to the reactor. The dynamic responses obtained were monitored by infrared analysis using the CH_4 peak at 3000 cm^{-1} and are illustrated in Fig. 6. A step increase in CO concentration is seen to produce a different response to a step decrease in concentration. When H_2 or a mixture of H_2 and CO were subjected to perturbations, similar responses were recorded, but these were independent of the direction of the step change. According to the analysis of Kobayashi (*5*) who classified the shape of transient response curves for simple reactions, inhibition by CO and competitive adsorption of the reactants H_2 and CO would account for the observed results.

In all of these experiments 0.2 g of the 1.5% Pt, 9% Ni catalyst, diluted with 0.8 g

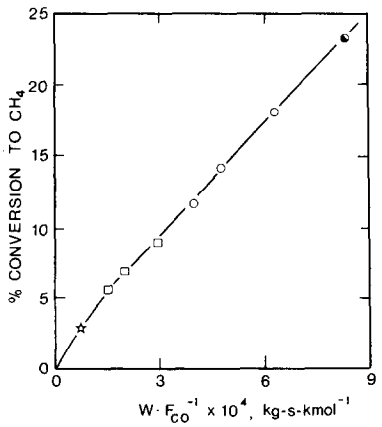

FIG. 5. Conversion as a function of the ratio catalyst mass/molar flow rate of CO (= W/F_{CO}). Temperature 270°C; pressure 0.205 MPa; H_2/CO = 3. (●) 0.710 g catalyst; (○) 0.501 g; (□) 0.251 g; (☆) 0.107 g.

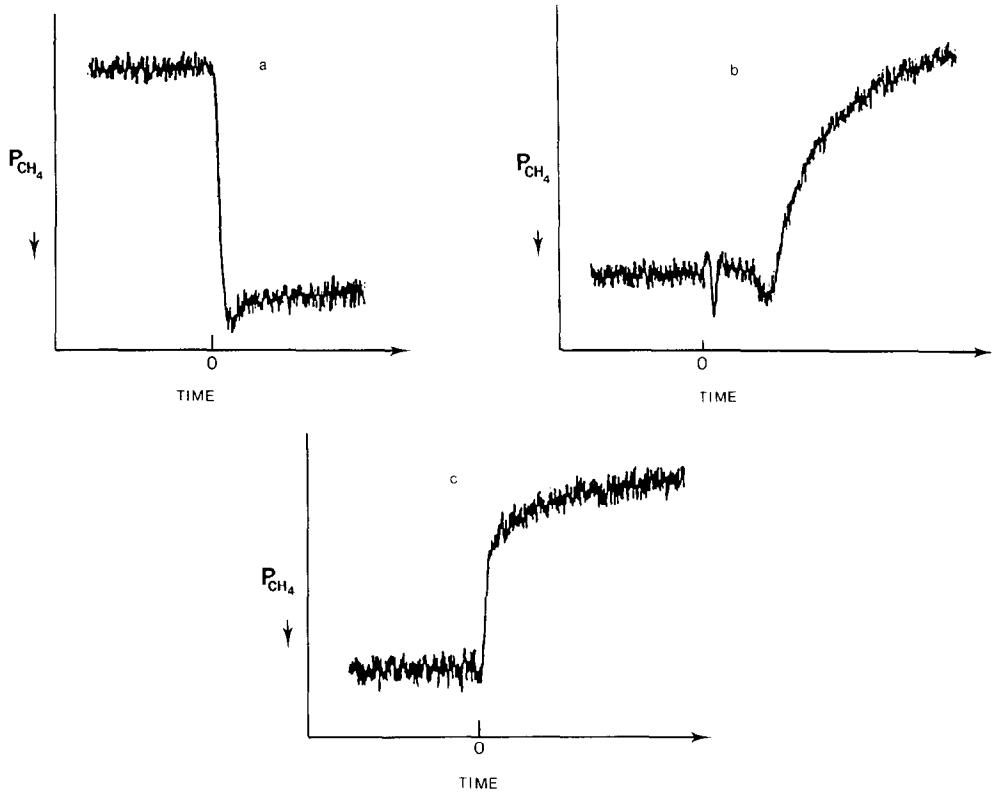

FIG. 6. Response to step changes in partial pressure. (a) Step increase $p_{CO} = 0 \rightarrow p_{CO} = 4.5$ kPa. (b) Step decrease $p_{CO} = 4.5$ kPa $\rightarrow p_{CO} = 0$. (c) Step decrease $p_{H_2} = 38.8$ kPa $\rightarrow p_{H_2} = 19.4$ kPa.

of alumina to assist heat dissipation, was used at a temperature and pressure of 300°C and 100 kPa respectively. The total flow rate was always constant. The feed gas compositions before and after the step change are given in Table 3.

Adsorption and Reaction at the Nickel Surface

By means of computer enhanced multiple reflectance infrared spectroscopy on a pure polished nickel surface, it was possible to observe both adsorption of reactants and methanation characteristics. A more detailed analysis of the infrared investigation has been reported elsewhere (*36*), but the main observations are incorporated here so that an overall mechanistic picture of methanation can be deduced.

Figure 7 shows that when a mixture of 9.3 kPa CO and 40 kPa H_2 is heated in a stepwise manner, an absorption band at 3250 cm^{-1} appears which gradually increases with increasing temperature. This

TABLE 3

Composition of Feed Gas for Dynamic Response Experiments

Fig. no.	Feed gas flowrate $cm^3\ min^{-1}$ STP	
	Initial	Final
6a	$H_2 = 75$	75
	CO = 25	25
	$N_2 = 485$	460
6b	$H_2 = 75$	75
	CO = 25	0
	$N_2 = 460$	485
6c	$H_2 = 200$	100
	CO = 15	15
	$N_2 = 300$	400

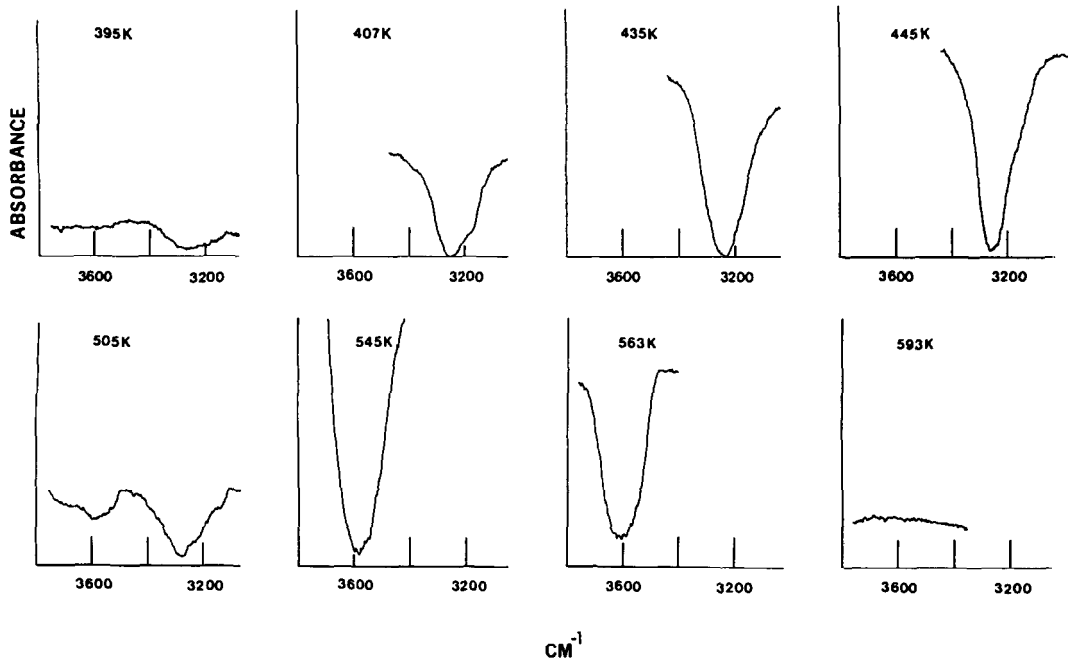

FIG. 7. Infrared spectra obtained on heating mixture of 0.093 bar CO and 0.40 bar H_2 on pure Ni plates.

band is assigned to Ni≡C—H on the grounds that a peak in an identical spectral position is obtained by the adsorption of 6.7 kPa C_2H_2 on freshly reduced Ni plates (*36*). At temperatures higher than 505 K, this species is hydrogenated to CH_4 and is confirmed by mass spectrometric analysis. The band at 3600 cm^{-1} is due to a surface OH species (*14*). Following its formation, it is hydrogenated to water after the Ni≡CH is removed.

Spectra obtained by the adsorption of 6.7 kPa CH_4 on freshly polished and reduced Ni plates are illustrated in Fig. 8. In Fig. 8a the band at 2963 cm^{-1} is due to Ni–CH_3 (*38*). The spectra in Figs. 8b–d were obtained after the addition of 40 kPa H_2 followed by stepwise heating. The bands at

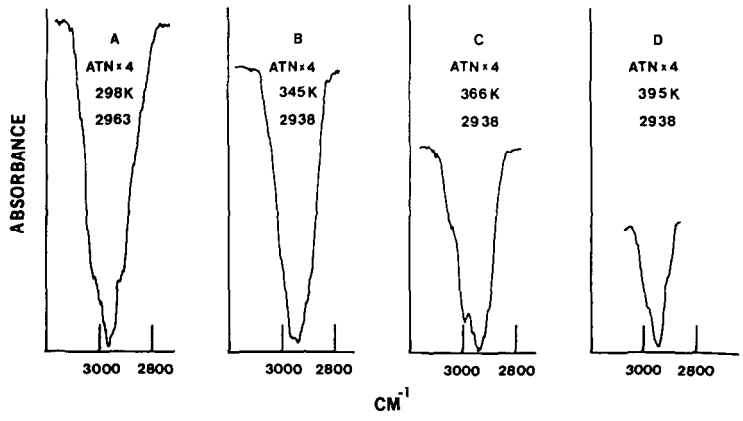

FIG. 8. Infrared spectra obtained on adsorption of 0.067 bar CH_4 on pure Ni plates.

FIG. 9. The 9% Ni catalyst totally deactivated by a methanation reaction.

FIG. 10. The 9% Ni, 1.5% Pt catalyst exposed to CO at 300°C.

2938 cm^{-1} are assigned to

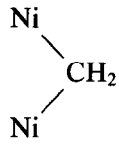

(*37, 38*) and are completely removed below 440 K at which temperature the band due to Ni≡CH is still increasing.

When clean Ni plates were heated in 9.3 kPa CO for 48 h at 423 K and cooled to room temperature, two bands at 1668 and 1440 cm^{-1} were obtained. These bands are assigned to $Ni(CO_3)^-$ as tabulated by Little (*14*). Exposure of only 1.3 kPa CO at 423 K to Ni for 3 h, followed by cooling at room temperature, also produced small bands at 1668 and 1440 cm^{-1}. On addition of 40 kPa H_2, followed by stepwise heating, two small bands at 3600 and 3250 cm^{-1} (ascribed to surface OH and Ni≡CH, respectively) appeared.

Physical Characteristics of the Catalyst Surface

Scanning electron microscopy of several catalyst samples revealed some interesting features of the surface morphology during methanation. All of the 9% Ni on alumina catalysts produced electron energy maps indicating a very high degree of dispersion of the nickel through the catalyst samples. Figure 9 shows part of the surface of a 9% Ni catalyst totally deactivated by a methanation reaction at 322°C. No massive carbon deposits appear and there is an absence of any kind of structured carbon such as whiskers or filaments. Several fresh and spent catalysts were examined by scanning electron microscopy and no structured carbon deposits were observed. This is in contrast to Fig. 10, which shows highly structured filamentous deposits of carbon obtained when a 9% Ni, 1.5% Pt on alumina catalyst was exposed to CO only at 300°C.

X-Ray photoelectron spectroscopy was also employed to examine the catalysts. Figure 11 is typical of the C(1*s*) spectra obtained. It can be deduced from the width of the C(1*s*) peak that more than one type of carbon species is present (*39*) in each of the five samples studied. Samples (a) and (b) were 29% Ni catalysts exposed to CO at 250°C; samples (c), (d), and (e) were 9% Ni catalysts employed during methanation. The observed electron energy distribution is different in sample (d) to the other samples, indicating a higher proportion of graphitic carbon present with a relatively high binding energy. The overall level of carbon observed was much higher for the catalysts exposed to CO disproportionation than those deactivated by methanation. A further interesting point is that the commercial catalyst samples displayed relatively high surface concentrations of Ca, Mg, and K; the Ca surface concentration was approximately threefold greater than Ni and the K surface concentration twice that of Ni.

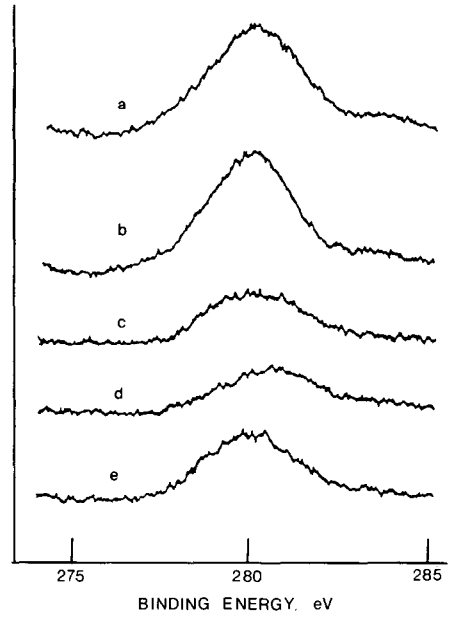

FIG. 11. Samples (a) and (b): 29% Ni commercial catalyst exposed to CO at 250°C. Samples (c), (d) and (e): 9% Ni catalyst after use during methanation.

DISCUSSION

Mechanism

Evidence accumulated from results of the various experimental investigations re-

ported provides an overall self-consistent model of the catalytic methanation process. Some of the mechanistic detail can be inferred from the reflectance infrared studies. It is suggested that the first methane precursor to appear is an Ni≡C—H complex which probably arises from

$$2Ni + CO_{(g)} \rightarrow Ni\text{–}C_{(ads)} + Ni\text{–}O_{(ads)}$$

followed by

$$Ni\text{–}C_{(ads)} + H_{(ads)} \rightarrow Ni{\equiv}C\text{—}H_{(ads)}.$$

It is well known that CO_2 is present in stoichiometric equilibrium mixtures of CO and H_2 (*3*) and is, as observed by us, a direct product of reaction. The infrared spectroscopic evidence points to its formation by

$$CO_{(g)} + Ni\text{–}O_{(ads)} \rightarrow CO_{2(g)} + Ni$$

the observed carbonate type bands at 1668 and 1440 cm^{-1} arising from

$$Ni\text{–}O_{(ads)} + CO_{2(g)} \rightarrow Ni\text{–}O\text{–}CO^{-}_{2(ads)}$$

when the sample cell is cooled. As this reaction occurred at temperatures below those at which the complex was formed, and recalling our earlier (*36*) observation that H_2 does not enhance the adsorption of CO, it therefore appears that the dissociation of CO is not influenced by the presence of H_2 and implies that the reaction

$$CO_{(g)} + H_{2(g)} \rightarrow C_{(ads)} + H_2O$$

does not occur during nickel catalyzed methanation. The gradual increase in amount of Ni≡C—H with increase in temperature and the eventual emergence of CH_4 as product (Fig. 7) suggests that CH_4 is formed by the stepwise addition of hydrogen to the surface Ni≡C—H complex. Since $NiCH_3$ and

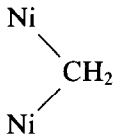

(observed when CH_4 is adsorbed on Ni in the presence of H_2) are removed by hydrogenation at a lower temperature than NiCH could be hydrogenated, it is possible that NiCH is the most abundant hydrocarbon species at the catalyst surface. This conclusion is in agreement with the recent work of Happel *et al.* (*40–42*), who showed, using isotopic labeling techniques, that $CH_{(ads)}$ is the most predominant reacting intermediate during methanation.

Water, also a principal product of reaction, could be formed by hydrogenation of the $Ni\text{–}OH_{(ads)}$ species (band at 3660 cm^{-1}),

$$Ni\text{–}OH_{(ads)} + \tfrac{1}{2}H_2 \rightarrow Ni + H_2O_{(g)}$$

As the $OH_{(ads)}$ spectrum was observed at temperatures higher than those necessary for complete NiCH hydrogenation, it is probable that there is a greater preponderance of surface hydroxyl than CH radicals. An experiment in which a stoichiometric feed of H_2 and CO ($H_2/CO = 3$) was passed over a 9% Ni on alumina catalyst at 533 K showed that when the CO feed was suddenly interrupted, CH_4 continued to be formed, but H_2O formation quickly ceased. Together with the observation that NiCH is in greater abundance than other hydrocarbon species, this indicates that the formation of Ni≡C—H is slow.

The evidence obtained from the dynamic response studies suggests that the surface reaction is the rate determining step, that hydrogen and carbon monoxide compete for adsorption and carbon monoxide inhibits the reaction.

Experiments in which the effects of products were observed show that water inhibits the rate, but that carbon dioxide and methane do not. This is compatible with the ir spectra, which show that water is much more strongly adsorbed than either methane or carbon dioxide.

Thus the probable mechanism of reaction is the competitive, dissociative chemisorption of CO and H_2, followed by stepwise hydrogenation of $O_{(ads)}$ and $C_{(ads)}$ to water and methane, respectively. The rate determining step for the conditions in this inves-

tigation appears to be the hydrogenation of active surface carbon.

The observations in this investigation lend support to the mechanism proposed by van Meerten *et al.* (*43*), albeit the rate determining step differs. Considering their observations and the work of Happel *et al.* (*40–42*) it seems probable that the rate determining step can change, depending on the experimental conditions. The most recent kinetic investigation of methanation (*44*) proposes a mechanism in which three third-order surface reactions occur. This is not supported by our observations and, indeed, is improbable on statistical grounds alone.

Modeling

The accumulated rate data were analyzed and fitted to an empirical power law model of the form

$$r = k p_{H_2}^{x} p_{CO}^{y} p_{H_2O}^{z}.$$

The partial pressure of water is included in the expression because it inhibits the reaction rate. On the other hand, methane is excluded, as it did not influence the rate. The exponents were determined individually by considering rate data in which only partial pressure varied. The final rate equation obtained is

$$r = 8.79 \exp\left(\frac{-9270}{T}\right) p_{H_2}^{1.27} p_{CO}^{-0.87} p_{H_2O}^{-0.13}$$

where the reaction rate is expressed in mol $s^{-1}g^{-1}$, the partial pressures in bar and temperature in degrees Kelvin. The activation energy corresponds to 78 kJ mol^{-1}. This is slightly lower than normally reported for methanation over nickel, and is probably the effect of the platinum promoter.

The standard deviation for this empirical kinetic expression is 16%, which compares favorably with the 13% reported by van Meerten *et al.* (*43*). Klose and Baerns (*44*) reported a standard deviation of 100%.

Models based on the postulated mechanism were derived using a Langmuir–Hinshelwood–Hougen–Watson (LHHW) approach, assuming one rate determining step with all other elementary steps in equilibrium. Models assuming the hydrogenation of surface carbon, hydrogenation of a CH surface complex and dissociation of chemisorbed hydrogen as alternative rate controlling steps did not match the observed kinetic results. None of the models derived, which included various assumptions about the abundance of surface species, gave good agreement between observed and predicted rates determined by nonlinear regression methods. Furthermore, the models are inconsistent with experimental observations relating to specific reaction orders with respect to particular reactants and products. It is not surprising that LHHW type models do not correlate the observed data, because the assumptions made (Langmuir adsorption, low total surface coverage, etc.) are invalid under steady-state methanation conditions.

Earlier kinetic models reported by other investigators are not in agreement with our experimental results. Two models (*24, 26*) include terms for reaction inhibition by CH_4, while other models (*24–26, 28, 45*) do not include terms for inhibition by water as observed in our investigation.

The two most recent investigations, by van Meerten *et al.* (*43*) and Klose and Baerns (*44*), are also not in agreement with the work reported here. Both sets of authors introduced further simplifications to the LHHW assumptions and derived quasi-empirical models. Van Meerten obtained a reasonable statistical fit for the hydrogenation of CH as the rate determining step, although this does not validate the proposed mechanism. Models derived using the same method for other rate determining steps also did not give acceptable correlations with our results.

Our conclusion is that a power rate law is the most reliable means of predicting reaction rates, provided that rates are not extrapolated outside the experimental boundaries.

Carbon Deposition

Active carbon fragments, produced during methanation when CO interacts with the catalyst surface, exist in different forms. Infrared reflectance studies (*36*), for example, show that long exposure of Ni to CO at about 425 K results in the formation of carbon which cannot be hydrogenated, while exposure of CO at relatively low partial pressures for shorter lengths of time gives rise to carbon which can be hydrogenated. The XPS spectra of the catalyst after methanation (Fig. 11) reveal broad carbon bands indicative of more than one carbon form. The carbon with the highest binding energy (approximately 280 eV) will have a more graphitic character than other forms present, although none of the carbon could be identified as wholly graphitic.

Experimental investigations employing the microcatalytic reactor also reveal the possibility of differing forms of carbon. The sudden decline in the activity of a promoted 9% Ni catalyst indicates that the surface properties have changed appreciably. Such a change in activity could be due to a phase transformation of the surface carbon fragments. This hypothesis is supported by the different conditions required for catalyst regeneration during the early and later stages of deactivation. In the early stages of the deactivation process complete regeneration could be achieved by treatment with H_2 at the same temperature at which methanation occurred. For longer periods of deactivation, however, activity could only be restored by treatment with H_2 at about 725 K. The exponential type of decay observed by us during the initial stages of deactivation (Fig. 2) has been invoked previously (*46*) in relation to coking during cracking reactions.

Pore volume distribution curves obtained for the deactivated catalysts suggest that extensive pore blockage does not occur. This is supported by the XPS spectra which indicate that the amount of surface carbon at total catalyst deactivation is relatively small. Furthermore, SEM indicates an absence of carbon filaments which can cause physical breakup of the catalyst. These observations all support the conclusion of a phase transformation of active surface carbon accounting for the deactivation.

The results of catalyst activity experiments illustrated in Fig. 3 show that preexposure of the 29% Ni catalyst to the methanation reaction at elevated temperatures reduces the activity at selected lower, but more usual, methanation temperatures. As the conversion of CO to CO_2 and CH_4 at each of the pretreatment temperatures was 100%, the deactivation process must be related to temperature. If surface carbon formation is the principal cause of deactivation, then the observed decline in activity resulting from high temperature pretreatment can be explained by a temperature-sensitive phase transformation of active carbon to a less active form. The presence of carbon at the catalyst surface at various stages of deactivation is confirmed by the presence of CO_2 in the effluent gases when mixtures of O_2 and N_2 are passed over the heated catalyst after use. The inability of the coprecipitated 29% Ni catalyst to reattain activity following treatment with H_2 after deactivation, suggests that the carbon deposited on the deactivated 29% Ni catalysts is much less reactive than the carbon on the surface of the deactivated impregnated catalysts.

These results correlate well with the carbon hydrogenation study of McCarty and Wise (*47*), who observed four types of surface carbon. These were classified by their reactivity toward hydrogen. The reactivity of the carbon could be altered by exposure to temperatures of the order of 350°C. Considering our results, it is probable that these observations are also consistent with an activated phase transformation of surface carbon.

Recent studies of carbon deposition during steam reforming over nickel indicate the presence of several surface carbon phases. Jackson *et al.* (*48*) observed an ac-

tive and inactive (to hydrogenation) phase, as well as filaments. The lack of filaments on our deactivated catalysts suggests that carbon filaments are not important in hydrogen rich environments, a conclusion supported by Gardner and Bartholomew (*49*).

ACKNOWLEDGMENTS

We are grateful to Professor M. W. Roberts (University College, Cardiff) for XPS analysis of five of our catalyst samples and to the SERC for provision of electron microscope facilities at the University of Bath. R. E. Hayes was the recipient of a Commonwealth Fund scholarship. The authors also acknowledge the helpful private communication of Professor J. Happel, Columbia University.

REFERENCES

1. Sabatier, P., and Senderens, J. B., *C.R. Acad. Sci.* **134,** 512 (1902).
2. Sabatier, P., and Senderens, J. B., *J. Chem. Soc.* **88,** 333 (1905).
3. Strelzoff, S., "Technology and Manufacture of Ammonia," Wiley, New York, 1981.
4. Watson, G. H., "Methanation Catalysts." IEA Coal Research Report, London, 1980.
5. Vannice, M. A., *Catal. Rev.* **14,** 153 (1976).
6. Vlasenko, V. M., and Yuzefovich, G. E., *Usp. Khim.* **39,** 1622 (1969).
7. Bousquet, J. L., Gravelle, P. C., and Teichner, S. J., *Bull. Soc. Chim.* **10,** 3693 (1972).
8. Fischer, F., and Tropsch, H., *Brennst-Chem.* **7,** 97 (1926).
9. Okamoto, Y., Nitta, Y., Imanaka, T., and Teranishi, S., *J. Catal.* **64,** 397 (1980).
10. Bell, A. T., *Catal. Rev.* **23,** 203 (1981).
11. Ponec, V., *Catal. Rev.* **18,** 151 (1978).
12. Araki, M., and Ponec, V., *J. Catal.* **44,** 439 (1976).
13. Wentrcek, P. R., Wood, B. J., and Wise, H., *J. Catal.* **43,** 363 (1976).
14. Little, L. H., "Infrared Spectra of Adsorbed Species." Academic Press, New York, 1966.
15. Blyholder, G., *J. Phys. Chem.* **68,** 2772 (1964).
16. Hayes, K. E., *Canad. J. Spec.* **25,** 81 (1980).
17. Mills, G. A., and Steffgen, F. W., *Catal. Rev.* **16,** 155 (1977).
18. Blyholder, G., and Neff, L. D., *J. Catal.* **2,** 138 (1963).
19. King, D. L., *J. Catal.* **61,** 77 (1980).
20. Dalla Betta, R. A., and Shelef, M., *J. Catal.* **49,** 383 (1977).
21. Ekerdt, J. G., and Bell, A. T., *J. Catal.* **58,** 170 (1979).
22. Inui, T., Hagiwara, T., and Takagami, Y., *Fuel* **61,** 537 (1982).
23. Bartholomew, C. H., Weatherbee, G. D., and Jarvi, G. A., *Chem. Eng. Commun.* **5,** 125 (1980).
24. Akers, W. W., and White, R. R., *Chem. Eng. Prog.* **44,** 553 (1948).
25. Weller, S., *AIChE J.* **2,** 59 (1956).
26. Lee, A. L., Feldkirchner, H. L., and Tajbl, D. G., *Amer. Chem. Soc. (Div. Fuel Chem.) Prepr.* **14,** 126 (1970).
27. Vannice, M. A., *J. Catal.* **37,** 462 (1975).
28. Vannice, M. A., *J. Catal.* **44,** 152 (1976).
29. Hayes, R. E., Ph.D. Thesis, University of Bath (1982).
30. Pritchard, P., *Dechema Monog.* **78,** 231 (1975).
31. Drmaj, D. T., and Hayes, K. E., *J. Catal.* **19,** 156 (1970).
32. Trimm, D. L., "Design of Industrial Catalysts." Elsevier, New York, 1979.
33. Somorjai, G. A., *Catal. Rev.* **23,** 189 (1981).
34. Mears, D. E., *Ind. Eng. Chem. Process Des. Dev.* **10,** 541 (1971).
35. Kobayashi, M., *Chem. Eng. Sci.* **37,** 343 (1982).
36. Hayes, R. E., Thomas, W. J., and Hayes, K. E., *Appl. Catal.* **6,** 53 (1983).
37. Pliskin, W. A., and Eischens, R. P., *J. Chem. Phys.* **24,** 482 (1956).
38. Blyholder, G., and Neff, L. D., *J. Catal.* **2,** 138 (1963).
39. Roberts, M. W., *Chem. Brit.* **17,** 510 (1981).
40. Happel, J., Suzuki, I., Kokayeff, P., and Fthenakis, V., *J. Catal.* **65,** 59 (1980).
41. Happel, J., Cheh, H. Y., Otarod, M., Ozawa, S., Severda, A. J., Yoshida, T., and Fthenakis, V., *J. Catal.* **75,** 314 (1982).
42. Otarod, M., Ozawa, S., Hin, F., Chew, M., Cheh, H. Y., and Happel, J., *J. Catal.* **84,** 156 (1983).
43. van Meerten, R. Z. C., Vollenbroek, J. G., de Croon, M.H. J. M., van Nisselrooy, P. F. M. T., and Coenen, J. W. E., *Appl. Catal.* **3,** 29 (1982).
44. Klose, J., and Baerns, M., *J. Catal.* **85,** 105 (1984).
45. Schoubye, P., *J. Catal.* **14,** 238 (1969).
46. Weekman, V. W., *Ind. Eng. Chem. Proc. Dev.* **7,** 90 (1968).
47. McCarty, J. G., and Wise, H., *J. Catal.* **57,** 406 (1979).
48. Jackson, S. D., Thomson, S. J., and Webb, G., *J. Catal.* **70,** 249 (1981).
49. Gardner, D. C., and Bartholomew, C. H., *Ind. Eng. Chem. Prod. Res. Dev.* **20,** 80 (1981).